Critical-state model with a secondary high-field peak in $J_c(B)$

T. H. Johansen, M. R. Koblischka, H. Bratsberg, and P. O. Hetland
Department of Physics, University of Oslo, P.O. Box 1048, Blindern, 0316 Oslo 3, Norway
(Received 14 January 1997; revised manuscript received 3 June 1997)

A critical-state model capable of describing the experimentally observed secondary or fishtail peak in magnetization data for bulk high-T_c superconductors is introduced. As suggested by a recent understanding of the fishtail effect, the field dependence of the critical current density is taken as a sum of two terms; one giving rise to a low-field magnetization peak and another being responsible for the fishtail peak. The model, which extends the Kim model by adding a Lorentzian term in $J_c(B)$, allows analytical treatment. Expressions for internal flux-density profiles as well as the various branches of the magnetization loop are presented. It is shown that measured magnetization loops of $NdBa_2Cu_3O_{7-\delta}$ samples showing a very pronounced fishtail peak are well fitted by this model. Using our procedure, $J_c(B)$ can be determined without invoking the Bean model (with a constant J_c), and thus avoiding an inconsistency in the analysis. [S0163-1829(97)02941-X]

I. INTRODUCTION

The fishtail effect (FE) or ''second peak anomaly'' found in magnetization loops is one of the still puzzling properties of high-T_c superconductors, found in several different materials. A common characteristic of all investigations is that the FE is observed only in *bulk* samples, either homogeneous or granular, and not in thin films of any material.[1–7]

A magnetization loop of a sample exhibiting the FE reveals two important features: (i) a minimum in magnetization, M, located close to the full penetration field, H^*, and (ii) a maximum in M at high fields. Usually, also a peak close to $H=0$, called the central or low-field peak, is present, as it is often found in strong-pinning, hard type-II superconductors. This central peak shrinks with raising temperature with the result that observed magnetization loops can have a wide variety of shapes.[4,6,7] It is obvious that the commonly used critical-state models with a monotonic field dependence in the critical current density, $J_c(B)$ like the Kim model,[8] the exponential model,[9] etc., are not well suited to properly characterize the FE.

Several attempts were made to ascribe the FE to the field-induced activation of a special pinning site like Y_2BaCuO_5 particles found in melt-processed $YBa_2Cu_3O_{7-\delta}$ samples.[10] However, only a quite general approach which is not sample or material specific, will be able to explain all features of the FE reported in literature, e.g., the scaling behavior of the magnetization around the fishtail peak,[6,11] the dynamic character of the fishtail minimum[12] or the FE in heavy-ion irradiated samples.[13]

A step towards a general model was made in Ref. 6 starting from the scaling of the magnetization loops and the change in relaxation behavior around the FE minimum. In this model, the shape of a FE magnetization loop is understood as a sum of two distinct contributions with quite different field and temperature dependencies. One of them is active only at low fields, thus being responsible for the formation of the central peak, and vanishes rapidly with increasing field. The high-field mechanism is developing with increasing field, and its maximum causes under certain conditions the fishtail peak. For the high-field part of the magnetization loops, a scaling of J_c, normalized to the maximum value at the FE peak, plotted versus $(1-T/T_c)^p$ $(p\approx 1.5-2)$ could be established.[6,7,11] This analysis was, as usually done in literature, based on the Bean model relation $J_c \propto \Delta M$, where ΔM is the width of the magnetization hysteresis loop. While this simple relation is a reasonable approximation for fields larger than H^*, the approach can easily give misleading results at fields lower than H^*,[14,15] thus complicating a proper analysis of the central peak and the low-field pinning mechanism. This problem is overcome if one instead fits the entire magnetization loop by a critical-state model based on a suitable function $J_c(B)$, which in this case should possess the characteristic FE features seen in experiments.

Based on these considerations, we suggest a model with $J_c(B)$ comprised of two additive terms, one monotonic part producing a central peak, and a second term representing the high-field peak. Such a separation is further motivated by recent experiments showing that it is possible to remove reversibly the FE by high-pressure oxygen loading of $YBa_2Cu_3O_{7-\delta}$ single crystals prepared in $BaZrO_3$ crucibles.[16]

In this paper we derive explicit expressions for both the ascending and descending field branches of the magnetization loop for this model, and make comparison with various FE shapes described in literature. We also show the fitting procedure applied to data obtained on $NdBa_2Cu_3O_{7-\delta}$ (NdBCO) samples.

II. OUTLINE OF THE MODEL

A form sufficiently general to allow parametrization of the variety of FE behaviors is the following extension of the Kim model:

$$J_c(B)=J_0\left[\frac{1}{1+|b|}+\frac{a}{(|b|-b_1)^2+b_2^2}\right], \tag{1}$$

with $b\equiv B/B_0$; J_0 and B_0 are the original parameters of the Kim model. The secondary peak is represented by the Lorentzian term characterized by its center position b_1, its

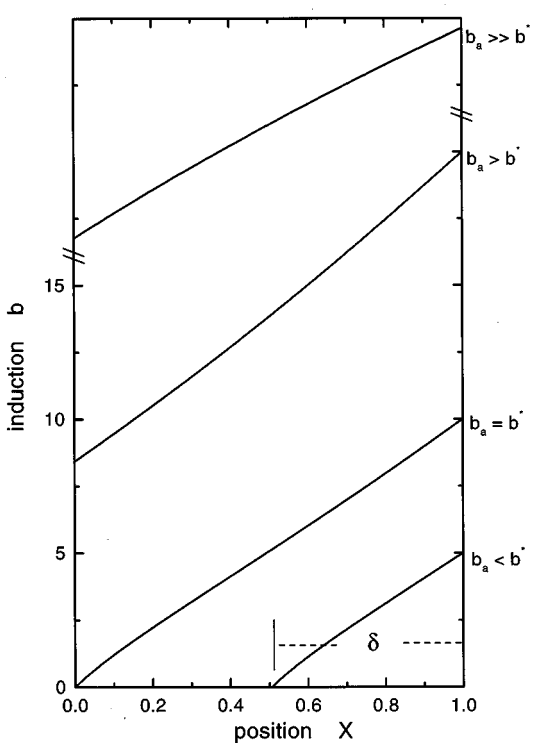

FIG. 1. Flux density profiles in one-half of the slab at various stages of penetration in an increasing applied field. $a=1000$, $b_1=b_2=25$, and $b^*=10$.

width b_2, and the relative amplitude a. All these parameters may depend on temperature. The Lorentzian form, which was motivated by the shape of the scaled magnetization loops presented in Ref. 6, has the additional advantage of permitting analytical calculations of flux density profiles and even M.

Consider a superconductor shaped as an infinite slab of thickness $2w$ placed in an external magnetic field, $\mathbf{H}=(B_a/\mu_0)\mathbf{z}$ directed parallel to the surface. The influence of a lower critical field and surface effects are neglected in the present treatment. Except for an interval immediately after the field sweep direction is reversed, which we omit in this calculation, the flux density profile $x(B)$ will always be a single-valued function wherever the current density $j_y \neq 0$. Thus, from Ampère's law, $j_y dx=-dB/\mu_0$, one can write the magnetization as[17]

$$\mu_0 M=-\int_{B_m}^{B_a} X\,dB, \tag{2}$$

where $X=x/w$ and B_m is the induction at the midplane, $x=0$. The flux profile is obtained by integrating Ampère's law, which gives

$$X=1+\frac{1}{\mu_0 w}\int_B^{B_a}\frac{dB'}{j_y(B')}. \tag{3}$$

Here $j_y(B)$ has the magnitude of the function, $J_c(B)$, and $\mathrm{sgn}(j_y)=-\mathrm{sgn}(dB/dx)$.

We consider first a zero-field cooled superconductor subjected to an increasing applied field. The flux then penetrates the slab in an outer layer of growing thickness δ, see Fig. 1. From Eq. (3) we obtain

$$X=1-\frac{(b_a+1)^2-(b+1)^2}{2k}+\frac{a}{k}\left[b_a-b+\frac{(u-1)^2-v^2}{v}\tan^{-1}\frac{v(b_a-b)}{(b_a+u)(b+u)+v^2}+(u-1)\ln\frac{(b+u)^2+v^2}{(b_a+u)^2+v^2}\right], \tag{4}$$

where $k=\mu_0 w J_0/B_0$, $u=a/2-b_1$, $v^2=b_2^2+a(b_1+1)-(a/2)^2$. Throughout this paper lower case b will denote induction values normalized by B_0, like $b_a=B_a/B_0$, etc. Interestingly, the function $X(b,b_a)$ consists of parts which are easily identified; the first being the well-known result of the Kim model, and the second being associated with the FE. From Eq. (2) it is clear that the same separation carries over to the expressions for M, as will become evident.

The flux penetration depth as function of the applied field follows directly from Eq. (4) as $\delta(b_a)=1-X(b=0,b_a)$. The initial stage with partial flux penetration lasts until b_a reaches the full penetration value b^*, which is given by $X(b=0,\ b_a=b^*)=0$.

Direct observation of flux density profiles is today possible with several experimental techniques like magneto-optic imaging,[18] Hall probe arrays,[19] etc. It is therefore of interest to look in some detail at the function $X(b,b_a)$. The graphs of Fig. 1 show how the flux density profile develops for an increasing applied field. In the initial stage the profile has a negative curvature, as in the original Kim model. Going beyond full penetration, the curvature is seen to change, with an intermediate region near $b_a=b^*$ where the profile has an S shape. Then, at even higher fields the curvature again becomes negative.

Calculation of magnetization gave the following results.

(i) $0\leqslant b_a\leqslant b^*$. The virgin branch of the magnetization curve is calculated from Eq. (2) with $B_m=0$, which yields

$$\frac{\mu_0 M}{B_0}=-b_a+\frac{b_a^2}{2k}+\frac{b_a^3}{3k}-\frac{a}{k}\left[2(1-u)b_a+\frac{b_a^2}{2}+\frac{p}{v}\tan^{-1}\frac{v b_a}{u b_a+u^2+v^2}+\frac{q}{2}\ln\frac{(b_a+u)^2+v^2}{u^2+v^2}\right], \tag{5}$$

where $p=-u+2u^2-u^3-2v^2+3uv^2$, and $q=1-4u+3u^2-v^2$. By expanding the RHS in powers of b_a one gets $-b_a+[1-a/(u^2+v^2)]b_a^2/2k+\cdots$, showing that the initial slope of the magnetization curve equals -1.

(ii) $b_a\geqslant b^*$. When the applied field exceeds the full penetration value the midplane induction becomes nonzero and dependent upon the applied field. We obtain $b_m(b_a)$ by setting $X=0$ in Eq. (4), which gives the relation $f(b_m)=2k$, where

$$f(b_m)=(b_a+1)^2-(b_m+1)^2-2a\left[b_a-b_m+\frac{(u-1)^2-v^2}{v}\tan^{-1}\frac{v(b_a-b_m)}{(b_a+u)(b_m+u)+v^2}+(u-1)\ln\frac{(b_m+u)^2+v^2}{(b_a+u)^2+v^2}\right]. \tag{6}$$

The magnetization then becomes

$$\frac{\mu_0 M}{B_0}=-b_a+\frac{b_a^2-b_m^2}{2k}+\frac{b_a^3-b_m^3}{3k}-\frac{a}{k}\left[2(1-u)(b_a-b_m)+\frac{b_a^2-b_m^2}{2}+\frac{p}{v}\tan^{-1}\frac{v(b_a-b_m)}{(b_a+u)(b_m+u)+v^2}+\frac{q}{2}\ln\frac{(b_a+u)^2+v^2}{(b_m+u)^2+v^2}\right], \tag{7}$$

which is valid until the field sweep is reversed. After a sufficient field reduction the induction gradient has changed sign throughout the slab, and the flux profile becomes again monotonic.

(iii) $b_a \geqslant 0$ and decreasing. From Eq. (3) one sees that changing the sign of j_y leads to a new profile function given by Eq. (4) only with the substitution $k \rightarrow -k$. Consequently, the same substitution also applies to the expression for the midplane field, which now is given by $f(b_m)=-2k$. We can immediately write the magnetization as

$$\frac{\mu_0 M}{B_0}=-b_a-\frac{b_a^2-b_m^2}{2k}-\frac{b_a^3-b_m^3}{3k}+\frac{a}{k}\left[2(1-u)(b_a-b_m)+\frac{b_a^2-b_m^2}{2}+\frac{p}{v}\tan^{-1}\frac{v(b_a-b_m)}{(b_a+u)(b_m+u)+v^2}+\frac{q}{2}\ln\frac{(b_a+u)^2+v^2}{(b_m+u)^2+v^2}\right]. \tag{8}$$

(iv) $-b^* \leqslant b_a \leqslant 0$. In this interval B changes sign at some position X_0, and since J_c depends upon $|b|$, two separate functions, $X^{(o)}(b)$ and $X^{(i)}(b)$, will describe the profile. In the outer region $X_0 \leqslant X \leqslant 1$ the profile $X^{(o)}$ has the same shape as during the initial stage, $0 \leqslant B_a \leqslant B^*$. Thus the contribution to M from the current distributed in this region is simply $-M_{\rm virgin}(-B_a)$, where $M_{\rm virgin}$ is given by Eq. (5). The induction profile in the inner region, $0 \leqslant X \leqslant X_0$, is found by integrating Ampere's law, $X^{(i)}=(\mu_0 w)^{-1}\int_B^{B_m} dB'/J_c$. Here the midplane induction, B_m, is determined by requiring $X_0=X^{(i)} \times (b=0)=1-\delta(-b_a)$, which is expressed by the relation

$$2k=(b_a-1)^2+(b_m+1)^2-2+2a\left[b_a-b_m+\frac{(u-1)^2-v^2}{v}\left(\tan^{-1}\frac{v b_a}{u^2-u b_a+v^2}-\tan^{-1}\frac{v b_m}{u^2+u b_m+v^2}\right)\right.$$
$$\left.+(u-1)\left(\ln\frac{(b_a-u)^2+v^2}{u^2+v^2}+\ln\frac{(b_m+u)^2+v^2}{u^2+v^2}\right)\right]. \tag{9}$$

The total magnetization can now be written as, $M=-M_{\rm virgin}(-b_a)+\int_0^{B_m} X^{(i)} dB/\mu_0$, or

$$M=-M_{\rm virgin}(-b_a)+M_{\rm virgin}(b_m)+b_m B_0/\mu_0. \tag{10}$$

(v) $b_a \leqslant -b^*$. In this range of b_a the situation is the same as for $b_a \geqslant b^*$, except now the direction of the supercurrent is reversed. In fact, the entire magnetization loop possesses the symmetry $M(-b_a)=-M(b_a)$.

III. FITS TO EXPERIMENTAL DATA AND DISCUSSION

Calculated magnetization loops for four different sets of model parameters are shown in Fig. 2. Figures 2(a)–2(d) show how the secondary peak may appear increasingly pronounced in the large-field hysteresis loop. In Fig. 2(a), the contribution of the Lorentzian term is switched off ($a=0$), yielding a purely Kim-type magnetization loop. Such a loop is indeed obtained after high-pressure oxygen loading of $YBa_2Cu_3O_{7-\delta}$ crystals prepared in $BaZrO_3$ crucibles.[16] These crystals are practically free of metallic impurities which are in conjunction with oxygen vacancy clusters responsible for the microscopic origin of the fishtail shape. As shown in Ref. 20, oxygen removal from these samples brings the FE shape gradually back. Figure 2(b) presents a magnetization loop with a small contribution from the Lorentzian term ($a=500$, $b_1=25$, and $b_2=35$), resulting in a shallow minimum and a small peak. Such loops are reported in literature for thin $DyBa_2Cu_3O_{7-\delta}$ single crystals (thickness about 15 μm) at temperatures around 40 K.[6,12,13,21,22] In (c), a well-developed FE is shown with a deep minimum and a high peak ($a=500$, $b_1=35$, and $b_2=25$). This situation can be found on several $RBa_2Cu_3O_{7-\delta}$ (R=rare earths) single crystals and melt-processed samples at temperatures above 60 K.[2,4,10,11] Finally, Fig. 2(d) shows a magnetization loop where the FE peak is dominating, and the low field peak gives only a minor contribution to the loop ($a=1500$, $b_1=35$, and $b_2=25$). This situation is encountered in relatively thick samples at elevated temperatures;[23] an example is given with the melt-processed $NdBa_2Cu_3O_{7-\delta}$ sample shown in Fig. 3. These various magnetization loops demonstrate clearly the flexibility of the model to simulate practically all shapes of the FE described in literature.

To demonstrate quantitatively how experimental magnetization loops can be fitted by the model, Fig. 3 presents measurements on two different $NdBa_2Cu_3O_{7-\delta}$ melt-processed samples with dimensions $1.92\times1.86\times0.3$ mm^3 (sample A) and $1.38\times1.18\times0.47$ mm^3 (sample B). Both samples show a $T_{c,\rm onset}$ of $\approx$94 K. The preparation procedure for these samples is described in Ref. 24. The magnetization loops are recorded using a superconducting quantum interference device magnetometer with the external field applied perpen-

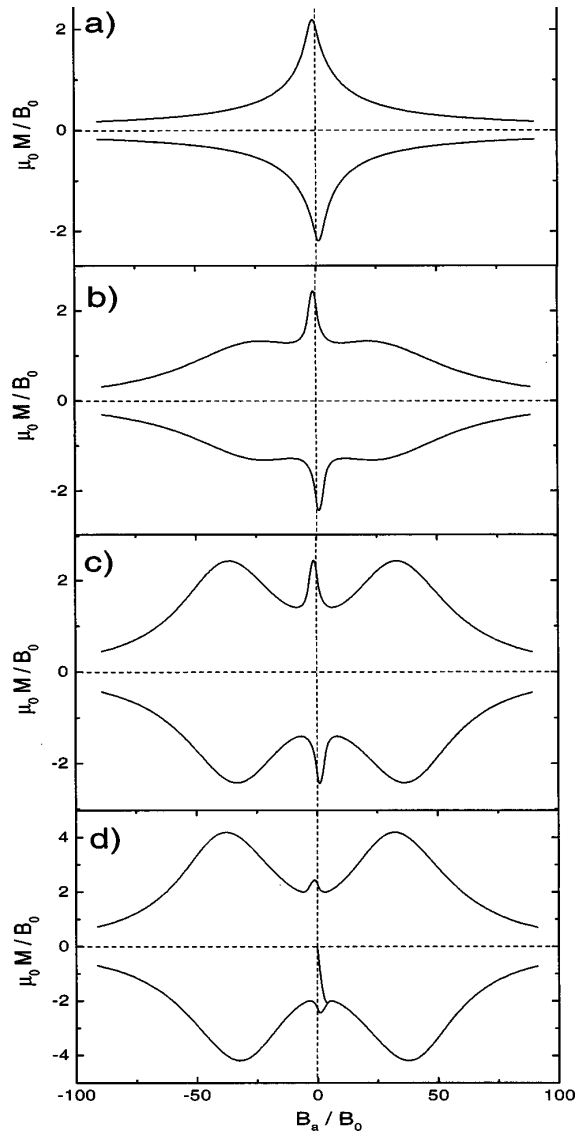

FIG. 2. Magnetization curves with ascending (negative M) and descending (positive M) field branches for four different sets of model parameters. (b) $a=500$, $b_1=25$, and $b_2=35$; (c) $a=500$, $b_1=35$ and $b_2=25$; and (d) $a=1500$, $b_1=35$; and $b_2=25$. For the widest hysteresis loop (d) also the virgin curve is plotted.

dicular to the sample surface. The experimental curves illustrate two different situations where a central peak is present (sample A, $T=74$ K), and a typical loop (sample B, $T=77$ K), where the central peak is nearly vanished (i.e., the peak width is smaller than the step size of the external field) and the irreversibility field is reached. To these data the model was best fitted using the following sets of parameters; $B_0=0.10$ T, $a=180$, $b_1=18$, $b_2=0.9b_1$, and $k=5.06$ (sample A), and $B_0=0.10$ T, $a=2000$, $b_1=11.5$, $b_2=0.9b_1$, and $k=0.07$ (sample B). The theoretical curves, drawn as full lines, clearly show that the present model is capable of describing the experimental magnetization loops very well. Only near the crossover into the reversible regime, which is not part of the model, the deviation becomes significant.

In Fig. 4 we have plotted the field dependence of the critical current density inferred from the magnetization fits.

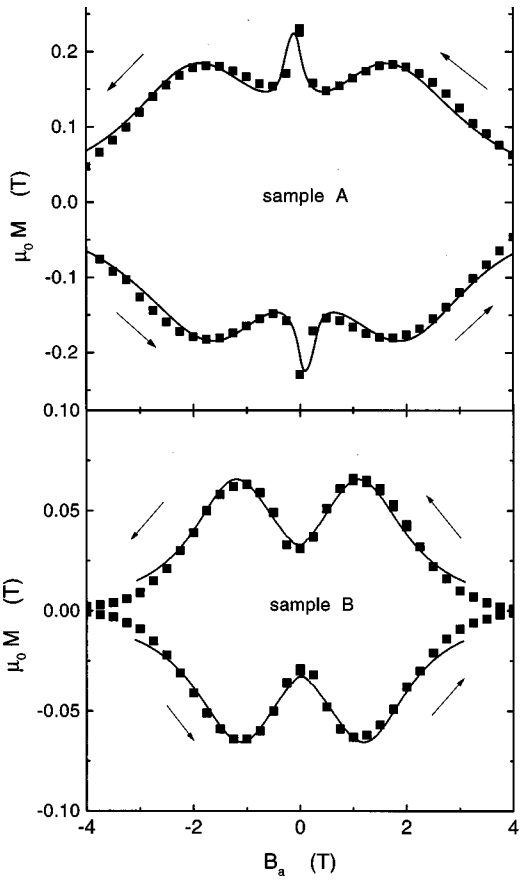

FIG. 3. Magnetization loops measured on two different $NdBa_2Cu_3O_{7-\delta}$ melt-processed samples fitted by the present critical state model [Eq. (1)]. The measurements illustrate two typical situations (upper, $T=74$ K, sample A; lower $T=77$ K; sample, B).

For sample A the $J_c(B)$ rapidly declines from a maximum value at $B=0$ to a local minimum near 0.5 T. While a similar behavior also follows if one assumes $J_c \propto \Delta M$, the strong deviation from Bean model behavior makes the quantitative result for the low-field peak significantly different. Figure 5 shows the low-field behavior of $J_c(B)$ for sample A obtained by the procedure advocated in the present work (graph 1), and by the usual Bean model interpretation (graph 2). The deviation between the two amounts to 40% near zero field. It then changes sign and grows to approximately 10% near 0.2 T. It is evident that the overall shape of the low-field peak in $J_c(B)$ is dramatically distorted when applying the Bean model formula, which from the outset is an inconsistent approach.

In the plot of Fig. 5 the full penetration field of $B^*=0.37$ T, another result coming out of our model fitting, is indicated. Above B^* the two different ways of determining $J_c(B)$ deviates much less. In fact, for $B_a \geqslant B^*$ the following general relation exists:[17]

$$\Delta M(B_a) = wJ_c(B_a)\left(1+\frac{1}{24}w^2\mu_0^2\frac{d^2}{dB_a^2}J_c^2(B_a)+\cdots\right). \tag{11}$$

When ΔM has a shape containing a pronounced FE peak, the second derivative in the correction term could become large.

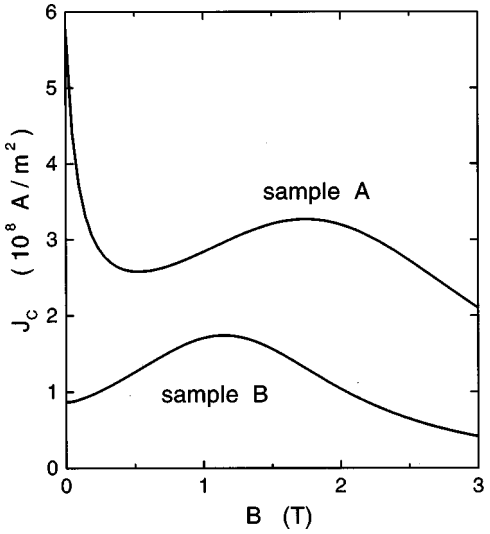

FIG. 4. Inferred field dependence of the critical current density for samples A and B.

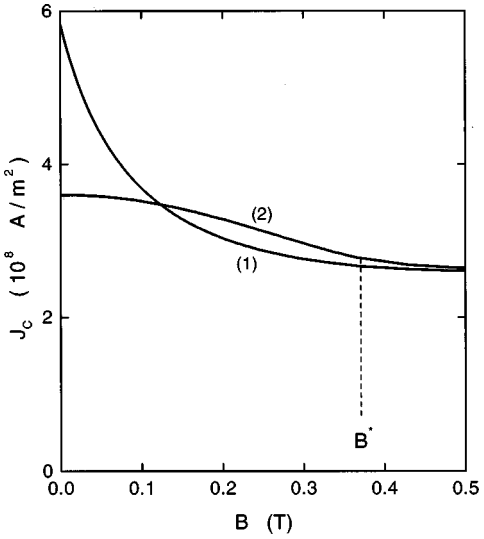

FIG. 5. Critical current density for sample A in the low-field region. Graph (1) is obtained by fitting the full magnetization loop with $J_c = J_c(B)$ as in Eq. (1). Graph (2) presents J_c inferred using the Bean model.

Thus, a simple Bean model interpretation can give significant errors also above B^*. It turns out, however, that for the parameters of sample A the usual Bean model interpretation deviates less than 4% in the high-field region.

In contrast to sample A, sample B, where a central peak is not present, shows the classical Bean behavior in the low-field region. Therefore, the errors produced by invoking the Bean model are much less in this case.

This analysis has shown that the B dependence of J_c for samples displaying the FE can be found in a consistent way by fitting a critical-state model to the full magnetization loop. In particular, when focus is set on the low-field behavior, e.g., to find scaling properties of the central peak and of the fishtail minimum, the procedure suggested in the present work avoids the severe misinterpretation produced by the Bean model formula when J_c has a strong field dependence at small fields.

IV. CONCLUSIONS

In conclusion, we have presented an extension of the critical state model in order to describe the fishtail phenomenon commonly found in bulk high-T_c superconductors. The derived expressions enable magnetization loops to be easily fitted. In this way $J_c(B)$ can be determined without invoking the Bean model (with a constant J_c), and thus avoiding an inconsistency in the analysis. Further work is planned with the aim of relating the experimentally observed scaling behavior of the FE to the temperature dependence of the parameters of the model, Eq. (1).

ACKNOWLEDGMENTS

The authors would like to thank Y. Galperin for stimulating discussions, and The Research Council of Norway for financial support. M.K. thanks M. Murakami for the hospitality during the stay at SRL/ISTEC, Tokyo, where the measurements were performed.

[1] M. Däumling, J. M. Seuntjens, and D. C. Larbalestier, Nature (London) **346**, 332 (1990); M. Osofsky, J. L. Cohn, E. F. Skelton, M. M. Miller, R. J. Soulen, Jr., S. A. Wolf, and T. Vanderah, Phys. Rev. B **45**, 4916 (1992).

[2] K. A. Delin, T. P. Orlando, E. J. McNiff, Jr., S. Foner, R. B. van Dover, L. F. Schneemeyer, and J. V. Waszczak, Phys. Rev. B **46**, 11 092 (1992); L. F. Cohen, J. R. Laverty, G. K. Perkins, A. D. Caplin, and W. Assmus, Cryogenics **33**, 352 (1993); Y. Yeshurun, N. Bontemps, L. Burlachkov, and A. Kapitulnik, Phys. Rev. B **49**, 1548 (1994); M. Werner, F. M. Sauerzopf, H. W. Weber, B. D. Veal, F. Licci, K. Winzer, and M. R. Koblischka, Physica C **235–240**, 2833 (1994); L. Klein, E. R. Yacoby, Y. Yeshurun, A. Erb, G. Müller-Vogt, V. Breit, and H. Wühl, Phys. Rev. B **49**, 4403 (1994).

[3] L. Civale, A. D. Marwick, T. K. Worthington, M. A. Kirk, J. R. Thompson, L. Krusin-Elbaum, Y. Sun, J. R. Clem, and F. Holtzberg, Phys. Rev. Lett. **67**, 648 (1991); L. Krusin-Elbaum, L. Civale, V. M. Vinokur, and F. Holtzberg, *ibid.* **69**, 2280 (1992).

[4] A. A. Zhukov, H. Küpfer, G. Perkins, L. F. Cohen, A. D. Caplin, S. A. Klestov, H. Claus, V. I. Voronkova, T. Wolf, and H. Wühl, Phys. Rev. B **51**, 12 704 (1995).

[5] Y. Abulafia, A. Shaulov, Y. Wolfus, R. Prozorov, L. Burlachkov, Y. Yeshurun, D. Majer, E. Zeldov, H. Wühl, V. B. Geshkenbein, and V. M. Vinokur, Phys. Rev. Lett. **77**, 1596 (1996).

[6] M. Jirsa, L. Půst, D. Dlouhy, and M. R. Koblischka, Phys. Rev. B **55**, 3276 (1997).

[7] M. R. Koblischka, A. J. J. van Dalen, T. Higuchi, K. Sawada, S.

I. Yoo, and M. Murakami, Phys. Rev. B **54**, R6893 (1996).
[8] Y. B. Kim, C. F. Hempstead, and A. R. Strnad, Phys. Rev. Lett. **9**, 306 (1962).
[9] W. A. Fietz, M. R. Beasley, J. Silcox, and W. W. Webb, Phys. Rev. **136**, 335 (1964).
[10] M. Ullrich, D. Müller, K. Heinemann, L. Niel, and H. C. Freyhardt, Appl. Phys. Lett. **63**, 406 (1993).
[11] G. K. Perkins, L. F. Cohen, A. A. Zhukov, and A. D. Caplin, Phys. Rev. B **51**, 8513 (1995); G. K. Perkins and A. D. Caplin, *ibid.* **54**, 12 551 (1996).
[12] A. J. J. van Dalen, M. R. Koblischka, R. Griessen, M. Jirsa, and G. Ravi Kumar, Physica C **250**, 265 (1995).
[13] M. R. Koblischka, A. J. J. van Dalen, Th. Schuster, M. Leghissa, and M. Jirsa, Physica C **235–240**, 2839 (1994).
[14] P. Chaddah, K. V. Bhagwat, and G. Ravikumar, Physica C **159**, 570 (1989).
[15] D.-X. Chen and R. B. Goldfarb, J. Appl. Phys. **66**, 2489 (1989).
[16] M. Däumling, E. Walker, J.-Y. Genoud, R. Flükiger, and A. Erb, Physica C **257**, 371 (1996).
[17] T. H. Johansen and H. Bratsberg, J. Appl. Phys. **77**, 3945 (1995); P. O. Hetland, T. H. Johansen, and H. Bratsberg, Cryogenics **36**, 41 (1996).
[18] M. R. Koblischka and R. J. Wijngaarden, Supercond. Sci. Technol. **8**, 199 (1995).
[19] E. Zeldov, D. Majer, M. Konczykowski, V. B. Geshkenbein, V. M. Vinokur, and H. Shtrikman, Nature (London) **375**, 373 (1995).
[20] A. Erb, J.-Y. Genoud, F. Marti, M. Däumling, E. Walker, and R. Flükiger, J. Low Temp. Phys. **105**, 1023 (1996); A. Erb, E. Walker, J.-Y. Genoud, and R. Flükiger, Physica C (to be published).
[21] M. Jirsa, A. J. J. van Dalen, M. R. Koblischka, G. Ravi Kumar, and R. Griessen, in *Proceedings of the 7th IWCC, 23.1.–28.1.94*, Alpbach, Austria, edited by H. W. Weber (World Scientific, Singapore, 1994), pp. 221–224.
[22] M. Jirsa, M. R. Koblischka, and A. J. J. van Dalen, Superlattices Microstruct. **21**, 335 (1997).
[23] S. I. Yoo, M. Murakami, N. Sakai, T. Higuchi, and S. Tanaka, Jpn. J. Appl. Phys., Part 2 **33**, L1000 (1994).
[24] M. Murakami, N. Sakai, T. Higuchi, and S. I. Yoo, Supercond. Sci. Technol. **9**, 1015 (1996).